Behavioral analysis of soil-straw movement in saline-alkali land during rotary tillage using discrete element method

Zhuang Zhao[1], Jialin Hou[1*], Dongwei Wang[2], Shuqi Shang[2], Peng Guo[1], Chao Xia[3]

(1. *College of Mechanical and Electronic Engineering, Shandong Agricultural University, Taian 271018, Shandong, China*;
2. *Yellow River Delta Intelligent Agricultural Machinery Equipment Industry Academy, Dongying 257300, Shandong, China*;
3. *College of Mechanical and Electronic Engineering, Xinjiang Agricultural University, Urumqi 830052, China*)

Abstract: Considering the problems of a low soil fragmentation rate and low straw mulching rate in the traditional rotary tiller tillage mode in the saline-alkali land, the layered stubble and soil crushing rotary tillage knife was designed, and the key structural parameters were determined by the analysis of rotary tillage knife-soil-straw movement. The soil-straw movement behavior in saline-alkali land under different working parameters of rotary tillage was analyzed, and the discrete element modeling of soil-straw-rotary tillage in saline-alkali land was established. In addition, the dynamic process of soil-straw aggregate fragmentation in saline-alkali land from a microscopic perspective was systematically explored. Combined with experimental optimization analysis, the optimum working parameters of the saline-alkali rotary tiller were obtained with a forward speed of 2.02 km/h, a working depth of 178.83 mm, and a rotation speed of 324.48 r/min. To verify the field performance of the machine, the soil fragmentation rate, straw burial rate, and tillage depth stability were chosen as test indices for the field trial. The average soil fragmentation rate was 91.85%, the average straw returning rate was 91.09%, and the average stability of tillage depth was 91.12%, indicating that the designed rotary tiller can effectively improve soil crushing and straw burial in saline-alkali land and meet the basic requirements of high-performance seedbed preparation in saline-alkali land.
Keywords: saline-alkali land, straw return, soil fragmentation, layered stubble and soil crushing.
DOI: 10.25165/j.ijabe.20251804.9349

Citation: Zhao Z, Hou J L, Wang D W, Shang S Q, Guo P, Xia C. Behavioral analysis of soil-straw movement in saline-alkali land during rotary tillage using discrete element method. Int J Agric & Biol Eng, 2025; 18(4): 38–52.

1 Introduction

Saline and alkaline land is an important reserve of arable land in China. There are 100 million hm^2 of saline and alkaline land resources in China, while only about 7.6 million hm^2 of saline and alkaline arable land can be directly utilized. The rational development and utilization of saline and alkaline land is of great significance to guarantee national food and oil security[1-4]. However, at present, the soil in saline soils is severely compacted, and the existing rotary tillers cannot be adapted to the characteristics of saline soils. There are problems of low soil fragmentation, high power consumption, and poor straw mulching during cultivation. Therefore, there is an urgent need for a high-performance seed bed preparation device that can be used in saline-alkali floor soil and high residue of wheat stubble[5-8].

At present, there is a lack of research on the interaction mechanism between tillage machinery, soil, and straw. Systematically exploring the movement laws and distribution effects of straw and soil under the action of different tillage machinery can help to fully understand the interaction mechanism between straw soil machinery, and is of great significance for optimizing the design of tillage machinery[9]. However, traditional experimental methods cannot determine the movement patterns of straw and soil due to complex factors such as soil properties and machine working parameters during the operation process[10,11]. The EDEM can assess the mechanisms of soil component-soil interaction and elucidate the dynamic processes in the soil[12,13]. Scholars, both domestic and international, have conducted numerous studies based on discrete elemental tillage modeling, mainly involving the assessment of post-tillage mechanical indices and the analysis of soil morphology and fine-scale displacements[14-16]. Saunders et al.[17] systematically analyzed the influence of parameters such as plough forward speed, operating depth, and soil entry angle on soil movement. Combined with field experiments, it was shown that EDEM can effectively evaluate soil movement mechanisms. Azimi-Nejadian et al.[18] analyzed the relationship between plough surface structural parameters and working parameters on weed burial performance and soil movement. They used a tracer for weed and soil identification, and experiments showed that EDEM could be a tool for optimizing the operational performance of soil-touching components. Torotwa et al.[19] conducted a study on the interaction between straw soil biomimetic discs in indoor soil troughs, and the results showed that compared to ordinary discs, biomimetic discs had lower tillage resistance and higher straw cutting efficiency. Farid et al.[20] conducted field experiments to study the grass burying effect of a plow with a grass blocking board, and pointed out that as the advancing speed decreases, the straw burying rate increases. Huang et al.[21] studied

Received date: 2024-08-31 **Accepted date:** 2025-03-10
Biographies: Zhuang Zhao, PhD, research interest: agricultural machinery and equipment, Email: 20192204158@stu.qau.edu.cn; **Dongwei Wang**, PhD, research interest: agricultural machinery and equipment, Email: w88030661@163.com; **Shuqi Shang**, PhD, research interest: agricultural machinery and equipment, Email: sqshang@qau.edu.com; **Peng Guo**, PhD, research interest: agricultural mechanization, Email: 1669753064@qq.com; **Chao Xia**, PhD, research interest: agricultural mechanization, Email: 20192204156@stu.qau.edu.cn.

***Corresponding author: Jialin Hou**, PhD, Professor, research interest: design and theory of agricultural equipment. College of Mechanical and Electronic Engineering, Shandong Agricultural University, Taian 271018, Shandong, China. Tel: +86-13605388153, Email: jlhou@sdau.edu.cn.

the interaction between device-soil-straw, and determined the optimal combination of structural parameters for the grass soil separation device based on field experiments. Guo et al.[22] conducted comparative field experiments and analysis on soil and straw displacement under two tillage methods of forward and reverse rotary tillage. The results showed that the soil and surface straw displacement of reverse rotary tillage was greater than that of forward rotary tillage. However, with the increase of blade rotation speed, the displacement of reverse rotary tillage decreased while that of forward rotary tillage increased. Xu et al.[23] investigated the influence of key operational parameters under the interaction of straw soil rotary tiller on straw displacement and burial effect. The results showed that the primary and secondary factors affecting straw burial rate and displacement were tillage depth, straw length, and cutter shaft speed.

In order to improve the efficiency and quality of cultivation in saline alkali land and clarify the dynamic relationship between rotary tiller-straw-soil, this paper designed layered stubble and soil crushing rotary tillage knife and realized the layered crushing of soil and straw, analyzing the saline soil-straw dynamics under different operating parameters of rotary tillers from a microscopic perspective. Combined with field performance verification tests, the optimal structural and operating parameters of the machine were determined, providing theoretical techniques and experimental solutions for the design and optimization of subsequent rotary tillers for the saline-alkali land.

2 Experiment materials and methods

2.1 Overall structure of layered stubble and soil crushing rotary tiller

As shown in Figure 1, the rotary tiller includes a soil breaking plow, three-point suspension, horizontal cover, transmission system, rotary tillage shaft, layered stubble and soil crushing rotary tillage knife, and so on. The layered stubble and soil crushing rotary tillage knife is mainly divided into the upper short-edged stubble knife and the lower long-edged soil crushing knife, which improves the efficiency of straw crushing and soil fragmentation rate in saline alkali land. During the operation, the rotary tillage knife carries out the straw-soil agglomerate crushing operation from far and near, from top to bottom, and the straw-soil agglomerate is crushed the second time from the action of the crushed soil cover plate so as to realize the soil crushing and the straw burying and mulching. The basic parameters of the rotary tiller are listed in Table 1.

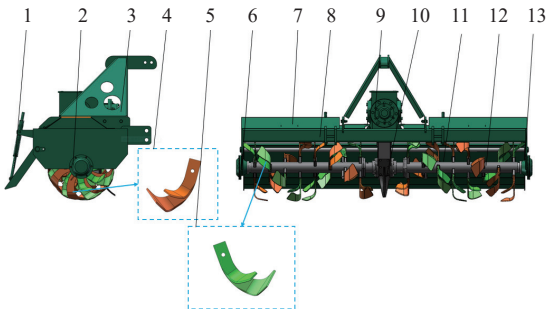

1. Soil breaking plow 2. Bearing compartment 3. Three-point suspension 4. Right rotary tillage blade 5. Left rotary tillage blade 6. Left side plate 7. Horizontal cover 8. Frame 9. Transmission system 10. Plow blade 11. Rotary tillage holder 12. Rotary tillage shaft 13. Right side plate

Figure 1 Mechanical structure of layered stubble and soil crushing rotary tiller

Table 1 Basic indicators of the rotary tiller

Parameters	Value
Dimension/mm	1050×2080×1150
Forward velocity/km·h^{-1}	1-5
Tillage depth of stubble knife/mm	0-220
Rotation speed of returnable knife/r·min^{-1}	280-340
Working width/mm	1800
Motive power/kW	≥90

2.2 Analysis of layered stubble and soil crushing rotary tillage blade-soil-straw dynamics

The layered stubble and soil crushing rotary tillage knife is mainly divided into the upper short-edged stubble knife and the lower long-edged soil crushing knife. To ensure the soil throwing performance and straw burial performance of the rotary tillage blades, the motion trajectories of the long-edged knife and the short-edged knife are trochoidal[24,25], as is shown in Figure 2. The motion trajectories of the long-edged knife endpoint M and the short-edged knife endpoint N were obtained.

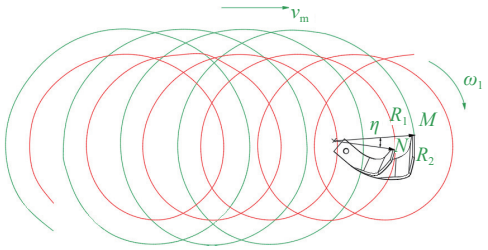

Note: v_m is the forward velocity of the implement, m/s; R_1 is the turning radius of the long-edged knife, mm; R_2 is the turning radius of the short-edged knife, mm; ω_1 is the angular velocity, rad/s; η is the phase angle between long-edged knife and short-edged knife.

Figure 2 Trajectory of layered stubble and soil crushing rotary tillage blade

$$\begin{cases} x_1 = v_m t + R_1 \cos(\omega_1 t) \\ y_1 = -R_1 \sin(\omega_1 t) \\ x_2 = v_m t + R_2 \cos(\omega_1 t + \eta) \\ y_2 = -R_2 \sin(\omega_1 t + \eta) \end{cases} \tag{1}$$

where, t is the working time of rotary tillage, s.

The absolute velocity of the long-edged knife endpoint M is:

$$v_M = \sqrt{v_{1x}^2 + v_{1y}^2} = \sqrt{v_m^2 + R_1^2\omega_1^2 - 2v_m R_1 \omega_1 \sin(\omega_1 t)} \tag{2}$$

The absolute velocity of the short-edged knife endpoint N is:

$$v_N = \sqrt{v_{2x}^2 + v_{2y}^2} = \sqrt{v_m^2 + R_2^2\omega_1^2 - 2v_m R_2 \omega_1 \sin(\omega_1 t)} \tag{3}$$

In the process of stubble crushing, the short-edged stubble cutter and the long-edged crushing knife need the characteristics of no entanglement, no soil, and low working resistance. Taking Q_1 and Q_2 as the stress points, the dynamic analysis of soil-straw aggregates is carried out, as shown in Figure 3.

$$\begin{cases} T_1 = N_1 \tan\tau_c \\ f_1 = \mu N_1 \\ \mu = \tan\varphi \\ T_1 > f_1 \end{cases} \tag{4}$$

where, τ_c is the dynamic sliding angle, (°); μ is the friction angle of soil-rotary tiller, (°); φ is the friction coefficient of soil-rotary tiller; T_1 is the tangential force of side cutting edge.

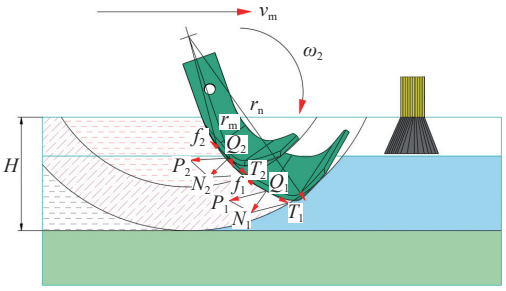

Note: ω_2 is the angular velocity, rad/s; r_m is the starting radius of the side cutting edge curve of long-edged soil crushing knife, mm; r_n is the termination radius of the side cutting edge curve of long-edged soil crushing knife, mm; H is the tilling depth, mm; N_1 is the normal reaction force on straw-soil from long-edged knife, N; N_2 is the normal reaction force on straw-soil from short-edged knife, N; T_1 is the normal force of side cutting edge curve of long-edged knife, N; T_2 is the normal force of side cutting edge curve of short-edged knife, N; P_1 is the tangential force of motion trajectory of long-edged knife, N; P_2 is the tangential force of motion trajectory of short-edged knife, N; f_1 is the friction force on straw-soil aggregates from long-edged knife, N; f_2 is the friction force on straw-soil aggregates from short-edged knife, N.

Figure 3 Dynamics analysis of soil cutting process

This paper takes the Q_1 point of the long-edged soil crushing knife as the object of study for the dynamics analysis. To reduce the working resistance of the layered soil cutting rotary tiller, it is necessary to reduce the normal force on the tangent blade curve and increase the tangential force on the tangent blade curve. The following conditions need to be met:

$$\begin{cases} f_1 < T_1 \\ \mu N_1 < N_1 \tan\tau_c \\ N_1 \tan\varphi < N_1 \tan\tau_c \\ \varphi < \tau_c \end{cases} \tag{5}$$

To ensure the sequential cutting of straw soil aggregates by the long-edged knife, the side cutting edge curve of the long-edged knife is selected as the sequential cutting-edge curves, which can further improve the soil fragmentation rate and reduce the working resistance during the cutting process. The equation of the side cutting edge curve was obtained.

$$r_a = \frac{r_n(r_m - H)}{(r_m - H)\cos K\varphi_\rho - \sqrt{r_n^2 - (r_m - H)^2 \sin K\varphi_\rho}} \tag{6}$$

where, r_a is the side cutting edge curve of long-edged knife; K is the static sliding angle decreasing ratio of long-edged knife edge curve; φ_ρ is the polar angle of side cutting edge curve, °.

Due to the depth of wheat straw ranging from 100-140 mm and the weed depth of 120-170 mm, in order to ensure effective cutting with the long-edged knife, the tillage depth of the long-edged knife is designed to be 180 mm, the turning radius is 250 mm, and the soil cutting pitch is 110 mm. Combining the results of the friction test, the friction factor between straw and steel is 0.68, and the friction angle is 34.53°. Therefore, the dynamic sliding cutting angle is greater than 34.53°, the starting point of the long-edged side cutting edge has a dynamic sliding cutting angle of 35°, and the ending point has a dynamic sliding cutting angle of 60°. The distance between two adjacent knives is 145 mm and the angle between two adjacent knives is 165°.

The short-edged knife side cutting curve adopts a positive rotation index curve, which can prevent straw weed entanglement, and the curve equation was obtained:

$$r_b = \rho_1 \left(\frac{\sin\tau_0}{\sin(\tau_0 - K\theta_1)} \right)^{\frac{1}{K}} \tag{7}$$

where, r_b is the side cutting edge curve of short-edged knife; K is the static sliding angle decreasing ratio of short-edged knife edge curve; ρ_1 is the polar radius of the short-edged knife edge curve, mm; τ_0 is the static sliding angle of short-edged knife, (°); θ_1 is the arbitrary polar angle of the short-edged knife edge curve.

The short-edged knife was designed with a tillage depth of 100 mm, a turning radius of 200 mm, a soil cutting pitch of 90 mm, and a starting radius of 110 mm for the side cutting edge curve. A static sliding cutting angle of 53° was determined for the side cutting edge, with a decreasing static sliding cutting angle ratio of 0.05.

The design standard for tangent-edged curves meets the requirements of soil turning performance while minimizing working resistance. To ensure that the working performance of the tangent-edge and the side cutting-edge of the layered stubble and soil crushing rotary tillage knife is the same and smoothly transitioned, the tangent-edge of the long-edged knife adopts the sequential cutting edge curves, and the tangent-edged curve of the short-edged knife adopts a positive rotation index curve.

In order to reduce the phenomenon of soil and grass entanglement between the tangent-edge of long-edged and short-edged knives, it is necessary to reduce the overlapping area between tangents as much as possible[26-28]. In this study, the working width of the tangent section of the long-edged knife B_1 is 95 mm, the working width of the tangent section of the short-edged knife B_2 is 75 mm, the bending radius of the long-edged knife ε is 60 mm, the bending radius of the short-edged knife ε_1 is 45 mm, the bent angle of long-edged knife is 75°, and the bent angle of short-edged knife is 65°, as shown in Figure 4.

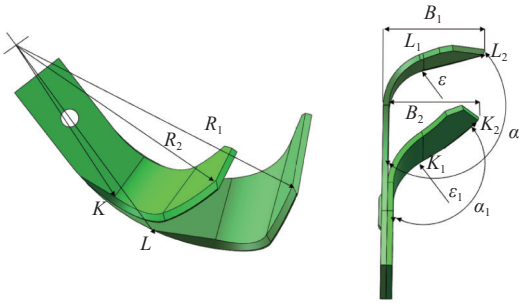

Note: B_1 is the working width of the tangent section of the long-edged knife, mm; B_2 is the working width of the tangent section of the short-edged knife, mm; ε is the bending radius of the long-edged knife, mm; ε_1 is the bending radius of the short-edged knife, mm; α is the bent angle of long-edged knife, (°); α_1 is the bent angle of short-edged knife, (°); L is the starting point of the side cutting edge of the long-edged knife; L_1 is the starting point of the tangent cutting edge of the long-edged knife; L_2 is the endpoint of the tangent cutting edge of the long-edged knife; K is the starting point of the side cutting edge of the short-edged knife; K_1 is the starting point of the tangent cutting edge of the short-edged knife; K_2 is the endpoint of the tangent cutting edge of the short-edged knife.

Figure 4 Overall structure of layered stubble and soil crushing rotary tillage

In order to further analyze the mechanism of straw-knife shaft twisting during rotary plowing process, a kinetic model of the straw entanglement process was established, as shown in Figure 5. It is assumed that wheat straw, weeds, and other tangles are wound side by side on the cutter shaft and that the tangles are uniform in thickness and tensile strength. The centrifugal force generated by the rotation of the cutter shaft is ignored.

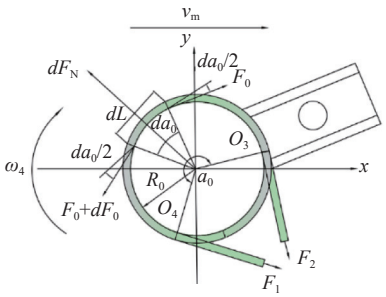

Note: dF_N is the positive pressure of the tool axis on the micro-arc segment, N; α_0 is the angle of wrapping corresponding to the wheat straw and weeds, (°); $d\alpha_0$ is the angle of wrapping corresponding to the micro-arc segment, (°); dF_0 is the tangential force of the tool axis on the micro-arc segment, N; F_0 is the tension at both ends of the micro-arc segment, N; ω_4 is the angular velocity, rad/s; R_0 is the inner diameter of cutter shaft, mm; O_3 and O_4 are the critical points for wheat straw and weed breakage, respectively; F_1 and F_2 are the critical tensile forces of wheat straw and weed breakage, respectively, N; dL is the length of straw wrapping material, mm.

Figure 5 Dynamic analysis of the grass twisting process of the cutter shaft

$$\begin{cases} dF_N = F_0 \sin\dfrac{d\alpha_0}{2} + (F_0 + dF_0)\sin\dfrac{d\alpha_0}{2} \\ fdF_N = (F_0 + dF_0)\cos\dfrac{d\alpha_0}{2} - F_0\cos\dfrac{d\alpha_0}{2} \end{cases} \tag{8}$$

where, fdF_N is the friction between knife shaft and wheat straw and weeds, N.

In this study, the microelement method is used to simplify the calculation.

$$\begin{cases} \sin\dfrac{d\alpha_0}{2} = \dfrac{d\alpha_0}{2} \\ \cos\dfrac{d\alpha_0}{2} = 1 \\ dF_0\left(\dfrac{d\alpha_0}{2}\right) \approx 0 \end{cases} \tag{9}$$

$$\begin{cases} \displaystyle\int_{F_2}^{F_1} \frac{dF_0}{F_0} = \int_0^{\alpha_0} f d\alpha_0 \\ F_1 = F_2 e^{f\frac{L}{R_0}} \end{cases} \tag{10}$$

where, L is the length of straw wrapping material, mm; f is the friction coefficient between straw and blade shaft.

$$S = 2\pi R_0 \tag{11}$$

where, S is the length of straw wrapping material, mm.

Combining Equation (10), the main factors affecting the winding of the rotary tiller blade shaft were identified as follows: length of straw wrapping material L, friction coefficient between straw and blade shaft f, and the radius of rotary tiller shaft. The height of weeds and wheat straw residues on the surface of saline alkali land is between 250-450 mm, and to avoid entanglement between the blade and roller, combined with Equation (11) the diameter of the rotary tillage blade shaft is 143 mm.

The rotary tiller is arranged in the manner of a double helix on the blade shaft in order to ensure that the congestion phenomenon does not occur on the adjacent rotary tillage knife cutting area. The design of the same cross-section of the arrangement of two rotary plow knives, the same cut soil area two rotary plow knives clamping angle of 180°, and the distance between the two neighboring rotary tillage knives installation is 113 mm. The rotary tillage knife arrangement is shown in Figure 6.

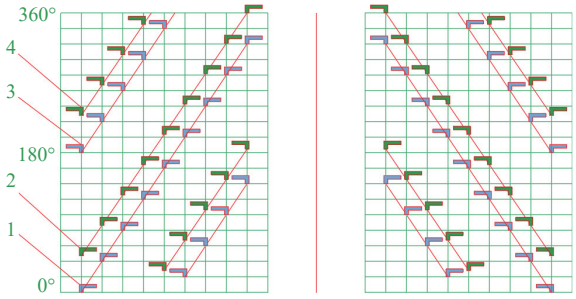

1. Right long-edged rotary tillage knife; 2. Right short-edged rotary tillage knife; 3. Left long-edged rotary tillage knife; 4. Left short-edged rotary tillage knife

Figure 6 Schematic diagram of rotary tillage knife arrangement

3 Discrete element simulation test

3.1 Soil particle discrete element modeling

This paper mainly focuses on discrete element modeling of saline soils in the Yellow River Delta region, investigating the distribution of salt content in saline alkali soil from 0-210 mm. The test results showed that the salinity of 0-70 mm saline soil was 1.5‰-2.5‰, which was a low salinity soil layer. The salinity of 70-140 mm saline soil was 2.5‰-3.5‰, which was a medium salinity soil layer, and the salinity of 140-210 mm saline soil was 3.5‰-5.5‰, which was a high salinity soil layer. The cultivated layer of saline alkali soil was divided according to the salt content level of different soil layers, with 0-70 mm defined as shallow soil, 70-140 mm as middle soil, and 140-210 mm as deep soil. The basic physical properties of saline soils are the basis for ensuring that the simulation test, such as soil density, soil moisture content, and soil firmness. The specific test results are listed in Table 2.

Table 2 Parameters of soil physical properties

Soil depth/mm	Soil density/g/cm³	Soil moisture content/%	Soil firmness/KPa
0-70	1.35	16.35	492.42
70-140	1.43	15.54	723.85
140-210	1.56	17.73	945.63
Mean value	1.45	16.54	720.63

Combined with the above analysis of the basic physical properties of the soil, this paper sets the radius of the soil particles as 5 mm. At the same time, it adopts the combination of discrete element particles to define the following three types of soil: single-grained soil model, double-grained soil model, and block soil model, as shown in Figure 7. To simulate the soil-soil fragmentation state during the actual rotary ploughing and stubble removal operation, this paper combines the previous research foundation of the research group[29,30], and the main contact parameters and physical properties of soil particles are determined, as listed in Table 3.

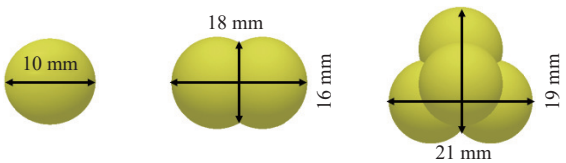

Figure 7 Soil discrete element particle model

3.2 Wheat straw particle discrete element modeling

In order to systematically analyze the basic physical properties of surface straw, a measurement area of 1 m×1 m was randomly selected for the measurement of wheat straw length and quality parameters. The test results are listed in Table 4.

Table 3 Soil discrete element model parameters

Parameters	Values
Soil density/kg·m^{-3}	1380
Soil Poisson's ratio	0.41
Shear modulus of soil/Pa	2.3×10^{6}
Coefficient of recovery of soil particles	0.59
Coefficient of static friction of soil particles	0.55
Coefficient of rolling friction of soil particles	0.13
Soil particle bonding radius/mm	5.20
Critical tangential stress of soil particles/Pa	2.0×10^{5}
Critical normal stress of soil particles/Pa	3.0×10^{5}
Soil particle tangential bond stiffness/N·m^{-1}	3.5×10^{6}
Soil particle normal bond stiffness/N·m^{-1}	2.3×10^{6}

Table 4 Parameters of straw physical properties of 1 m²

Type	Range of lengths/mm	Average length/mm	Dimensions of long axis/mm	Dimensions of short axis/mm	Average mass/g
A	0-50	48.5	8.5	3.2	384.75
B	50-150	114.6	18.3	11.4	172.48
C	150-200	173.7	22.5	13.7	86.82
D	200-250	228.4	24.8	16.5	73.21

According to the basic physical parameters of straw in Table 4, four different types of straw discrete metamodels were established, as shown in Figure 8. In order to simulate the dynamic desorption relationship between straw and soil, the straw-soil discrete element bonding model was established, in which the particle bonding radius is 2 mm. Combined with the previous research foundation of the research group and related research[31–34], the main contact parameters and physical properties of straw were determined, as listed in Table 5.

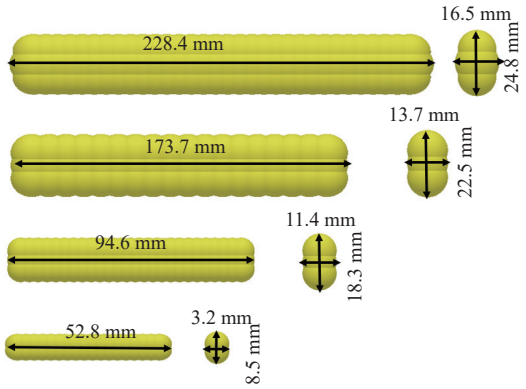

Figure 8 Discrete meta-model of wheat straw

Table 5 Wheat straw element model parameters

Parameters	Values
Wheat straw density/kg·m^{-3}	235
Wheat straw Poisson's ratio	0.39
Shear modulus of wheat straw/Pa	1.0×10^{6}
Coefficient of recovery of wheat straw	0.43
Coefficient of static friction of wheat straw	0.11
Coefficient of rolling friction of wheat straw	0.05
Wheat straw particle bonding radius/mm	3.50
Critical tangential stress of wheat straw/Pa	6.0×10^{5}
Critical normal stress of wheat straw/Pa	4.0×10^{5}
Wheat straw particle tangential bond stiffness/N·m^{-1}	5.5×10^{6}
Wheat straw particle normal bond stiffness/N·m^{-1}	4.3×10^{6}

3.3 Discrete element modeling of soil-straw

As shown in Figure 9, to meet the actual operating conditions, a discrete element model of straw-soil agglomerate was established in this paper. The dimensions of the soil bin are 2100 mm× 2000 mm×210 mm, and the total number of soil particles is 500 000. Meanwhile, the mass of straw type A is 1539 g, the mass of straw type B is 659.92 g, the mass of straw type C is 347.28 g, and the mass of straw type D is 292.84 g. To ensure the accuracy of the simulation test, the experimental simulation step was set to 3.1×10^{-6}, the grid cell size was set to 3 mm, and the data acquisition time interval was set to 0.01 s[35–39]. At the same time, the three-dimensional model of the rotary tiller was saved in IGS format and imported into the discrete element model of straw-soil agglomerate for the working parameter settings[40–43] according to GB/T5668-2017, in which the forward speed was 1 km/h, the rotational speed of the cutter shaft was 280 r/min, and the working depth was 160 mm for the rotary tillage and stubble test of wheat straw; the total simulation time is 5.5 s. Combined with additional references[44–46], the main contact parameters and physical properties of the rotary tiller were determined, as listed in Table 6. To investigate the straw-soil movement law in the test process, this paper selects six rows of straw from L_1-L_6 as well as shallow soil 0-70 mm, middle soil 70-140 mm, and deep soil 140-210 mm for dynamic analysis of the stubble crushing operation process.

3.4 Analysis of dynamic relationship between rotary tiller-soil-straw

This paper systematically investigates the relationship between soil-straw dynamics at different depths under the action of layered stubble and crushing soil rotary tillage. The short-edged rotary tillage knife mainly breaks up and transports wheat straw, shallow

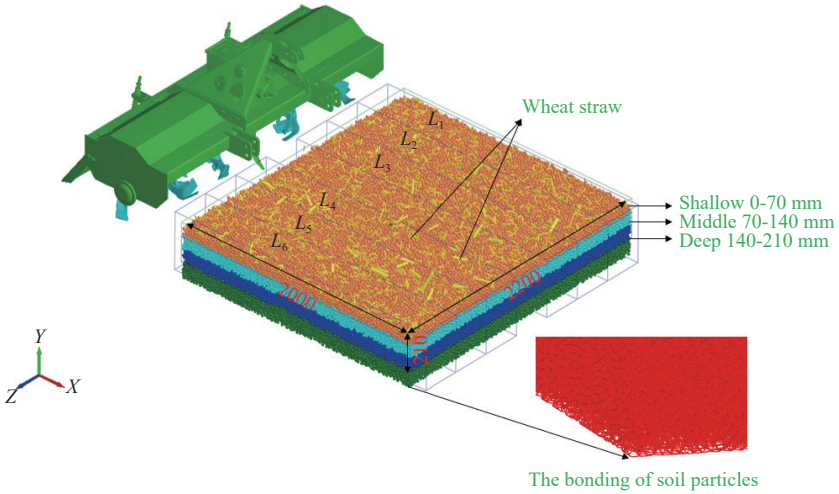

Figure 9 Discrete meta-model of soil-straw-rotary tillage knife

Table 6 Rotary tillage knife-soil contact parameters

Parameters	Values
Rotary tillage knife density/kg·m^{-3}	7801
Rotary tillage knife shear modulus/Pa	7.97×10^{10}
Poisson's ratio of the rotary tillage knife	0.3
Rotary tillage knife-soil recovery coefficient	0.64
Rotary tillage knife-soil static friction coefficient	0.18
Rotary tillage knife-soil rolling friction coefficient	0.57
Recovery coefficient of soil-straw	0.13
Static friction coefficient of soil-straw	0.46
Rolling friction of soil-straw	0.01
Rotary tillage knife-straw recovery coefficient	0.58
Rotary tillage knife-straw static friction factor	0.37
Coefficient of rolling friction rotary tillage knife-rotary tillage knife	0.02

soil, and medium soil. In an operation cycle, the short-edged rotary tiller knife crushes the straw firstly in the process of compound movement, and then crushes the saline shallow soil and the middle soil aggregates in turn. At the same time, the straw-soil is thrown backward in the direction of the tangent line at the endpoint of the short-edged rotary tiller knife. The long-edged rotary cutter mainly carries out the crushing and transportation of the saline-alkaline middle soil and deep soil aggregates, and at the same time, it cooperates with the short-edged rotary cutter to complete the burial of wheat straw. As shown in Figure 10 and Figure 11, the soil velocity and force changes at different depths are systematically demonstrated from a microscopic point of view, and the particle velocity and force limit of saline alkali soil are mainly concentrated at the contact position between the rotary tiller and the soil.

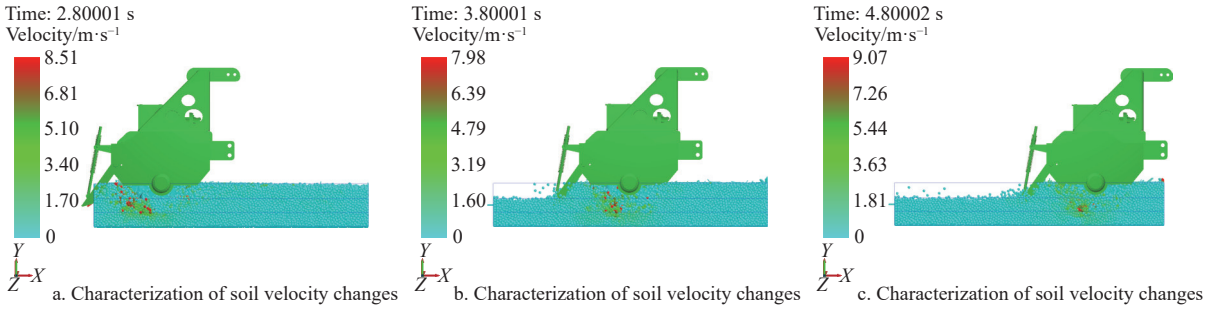

a. Characterization of soil velocity changes in saline soils at the 2.8 s simulation moment

b. Characterization of soil velocity changes in saline soils at the 3.8 s simulation moment

c. Characterization of soil velocity changes in saline soils at the 4.8 s simulation moment

Figure 10 Characteristics of soil velocity changes at different simulation times

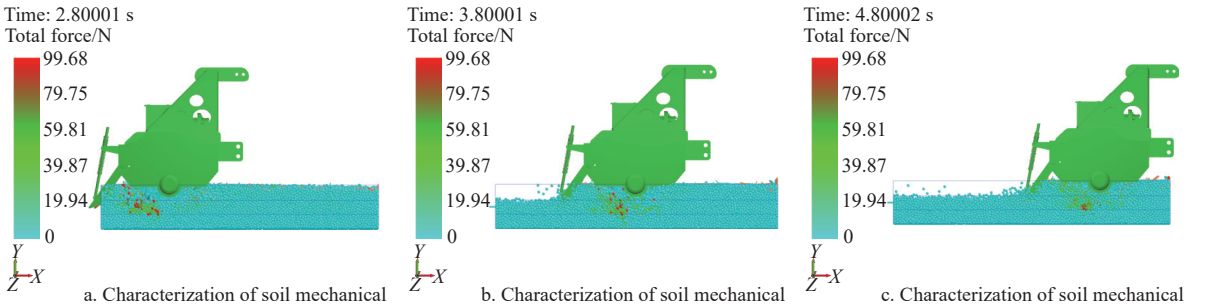

a. Characterization of soil mechanical properties changes in saline soils at the 2.8 s simulation moment

b. Characterization of soil mechanical properties changes in saline soils at the 3.8 s simulation moment

c. Characterization of soil mechanical properties changes in saline soils at the 4.8 s simulation moment

Figure 11 Characteristics of soil force changes at different simulation times

To investigate the influence of different salt content levels in saline alkali land on rotary tillage performance, this article investigates the effects of rotary tillage blades on tillage performance at salt content levels of 1.5‰-5.5‰. Setting the rotary tiller operating depth to 140 mm, the rotational speed of the cutter shaft to 280 r/min, the forward speed to 3 km/h, and the quality of wheat straw at 800 g/m^2, the experimental results are shown in Figure 12. For the soil fragmentation rate, with the increase of soil salinity, when the soil salinity is within the range of 1.5‰-3.5‰, the change in soil fragmentation rate is not significant. When the soil salinity is within the range of 3.5‰-5.5‰, soil fragmentation rate gradually decreases, with the maximum year-on-year decrease at 9.44%. This may be due to the increase in soil salinity, which leads to an increase in the compactness of soil straw aggregates. For the wheat straw return rate, when the soil salinity is within the range of 1.5‰-3.5‰, the wheat straw return rate gradually increases, and the maximum value is 91.24%. When the soil salinity is within the range of 3.5 ‰-5.5 ‰, the wheat straw return rate gradually decreases, and the maximum year-on-year decrease was 7.42%. This may be due to the decrease in soil fragmentation rate in saline alkali land, which decreases the rate of returning straw to the field.

This paper systematically explores the process of wheat straw fragmentation and burial at different simulation times from the microscopic perspective. As shown in Figure 13, the change law of

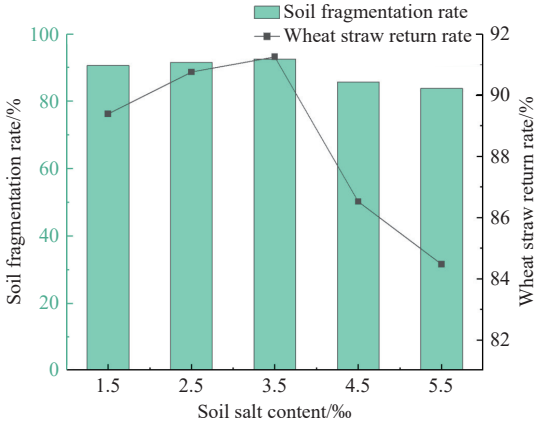

Figure 12 Influence of soil salinity on tillage performance

wheat straw velocity within 0-5 s and the straw burying situation after operation was analyzed. In one operation cycle, wheat straw realizes the whole process of crushing-displacing-burying under the action of short-edged rotary tillage knives, and the highest velocity of wheat straw was concentrated at the tip of the short-edged rotary blade. In the simulation test interval of 3-5 s, the mulching of wheat straw was realized under the coordinated operation of short-edged and long-edged rotary knives, and the mulching depth ranged from 5-10 cm. As shown in Figure 14, the wheat straw mechanics change law and velocity change law at different simulation times are similar, and the straw force maximum area is mainly concentrated in the short-edged rotary blade operation area.

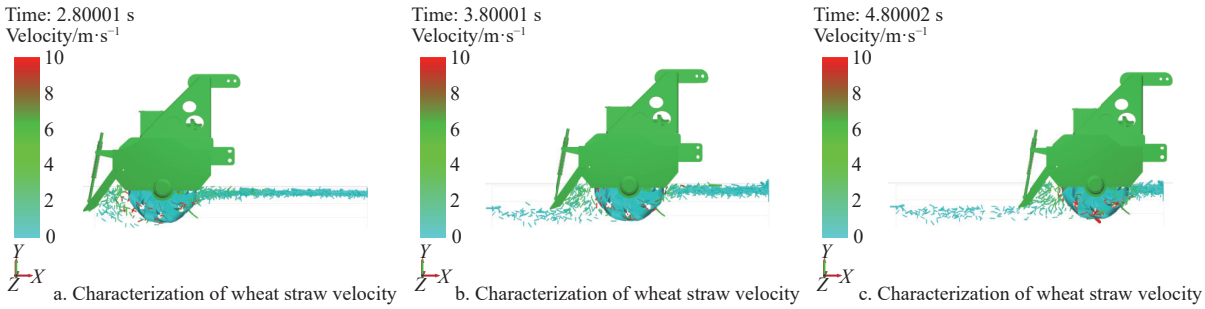

a. Characterization of wheat straw velocity changes in saline soils at the 2.8 s simulation moment

b. Characterization of wheat straw velocity changes in saline soils at the 3.8 s simulation moment

c. Characterization of wheat straw velocity changes in saline soils at the 4.8 s simulation moment

Figure 13 Characteristics of wheat straw velocity changes at different simulation times

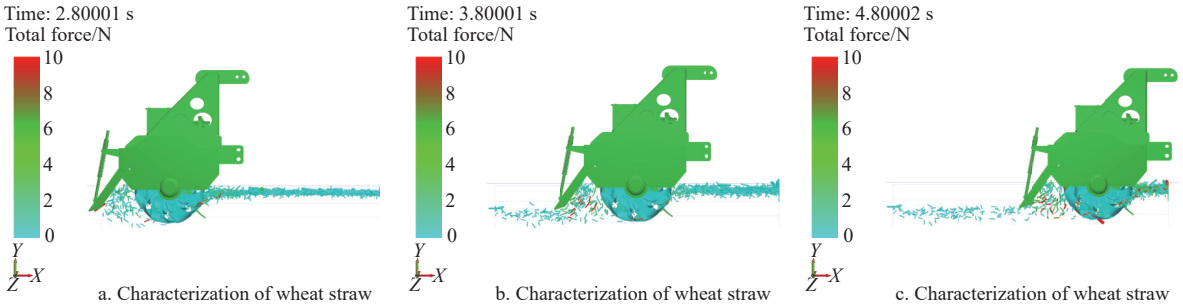

a. Characterization of wheat straw mechanical properties changes in saline soils at the 2.8 s simulation moment

b. Characterization of wheat straw mechanical properties changes in saline soils at the 3.8 s simulation moment

c. Characterization of wheat straw mechanical properties changes in saline soils at the 4.8 s simulation moment

Figure 14 Characteristics of wheat straw force changes at different simulation times

Setting the rotary tiller operating depth to 140 mm, the rotational speed of the cutter shaft is 280 r/min, the forward speed is 3 km/h, and the salt content level is 1.5 ‰. To investigate the influence of different wheat straw content in saline alkali land on rotary tillage performance, this article investigates the effects of rotary tillage blades on tillage performance at wheat straw contents of 800 g/m², 1000 g/m², 1200 g/m², 1400 g/m², and 1600 g/m²; the experimental results are shown in Figure 15.

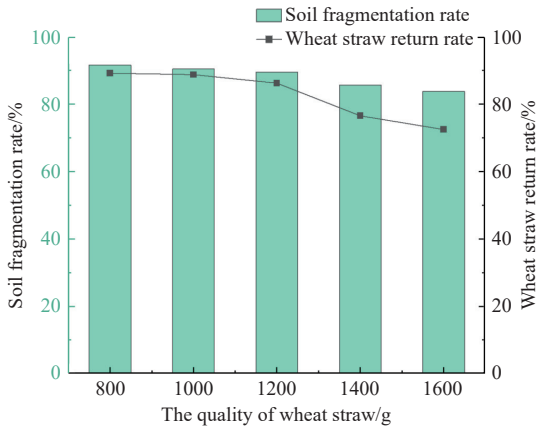

Figure 15 Influence of quality of wheat straw on tillage performance

For the soil fragmentation rate, with the increase of wheat straw content, when the quality of wheat straw is within the range of 800-1200 g/m², the change in soil fragmentation rate is not significant. When the quality of wheat straw is within the range of 1200-1600 g/m², the soil fragmentation rate gradually decreases, and the maximum year-on-year decrease was 8.55%. For the wheat straw return rate, when the quality of wheat straw is within the range of 800-1200 g/m², the wheat straw return rate gradually decreases. The maximum value is 89.18%, and the maximum year-on-year decrease was 18.73%. When the quality of wheat straw is within the range of 1200-1600 g/m², the wheat straw return rate also gradually decreases.

In order to investigate the relationship between soil movement and mechanical properties at different depths during the test, this paper systematically analyzes the change rule of velocity and force in shallow, middle, and deep soil layers. Between 2-2.5 s, the rotary plough knife disturbed the shallow soil, middle soil, and deep soil, and the soil produced a tendency of movement under the compound movement of the rotary plough knife. As shown in Figure 16, between 2.5 and 3.0 s, the soil velocity and force showed an upward trend. In contrast, the soil in each layer moved in the tangential direction of the endpoint of the rotary cutter. Between 3.0 and 5.0 s, the force and velocity of each layer were in the dynamic stabilization stage. Between 5.0 and 6.0 s, with the end of the simulation test, the force and velocity of each layer gradually tended to 0. The degree of soil disturbance during the whole simulation test was as follows: shallow soil>middle soil>deep soil.

To analyze the motion and mechanical properties of the straw at different moments during the test, this paper systematically analyzes the change rule of velocity and force of the straw from L_1

to L_6. As shown in Figure 17, between 2-2.5 s, under the action of soil disturbance, the straw was subjected to soil static friction to produce an upward movement tendency, and at this time, the straw was in a stationary state. Between 2.5 and 5.0 s, the degree of straw disturbance gradually increased. Because the rotary tillage knife adopts a double helix shape mounted on the cutter shaft, the rotary tillage knife acted alternately on the straws of L_1-L_6, and the peaks of the force and speed of the straws of each row appeared alternately. Between 5.0 and 6.0 s, the simulation test ended, and the straw force and velocity gradually tended to 0.

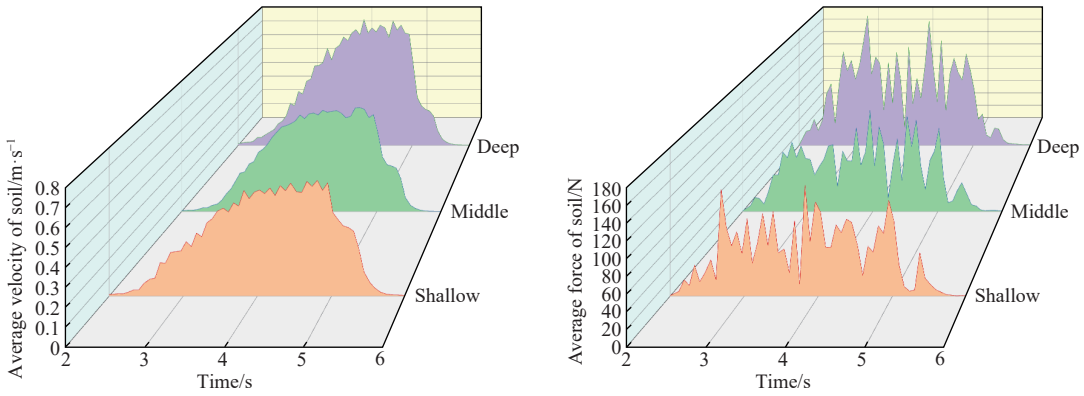

Figure 16 Mean velocity-force variation patterns of saline soils at different depths

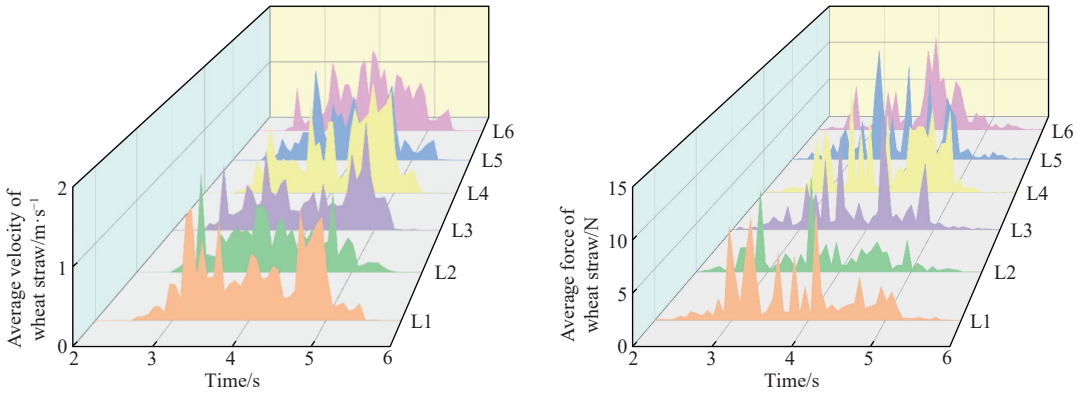

Figure 17 Mean velocity-force variation patterns of wheat straw

3.5 Analysis and discussion of simulation tests

To investigate the dynamic relationship of layered stubble and crushing soil rotary tillage on straw-soil, this paper adopts the one-factor method to systematically analyze the straw-soil disturbance law. In order to improve the crushing efficiency of soil-straw aggregates in saline-alkali land, and combined with the above theoretical analysis and practical operation requirements, the range of values for the forward speed is determined as 1-5 km/h; the range of values for the working depth is 140-180 mm; and the range of values for the cutter speed is 280-340 r/min. This paper takes the dynamic characteristics of L_1, L_3, and L_5 wheat straw and the shallow, middle, and deep soil as the test indices to systematically investigate the influence of the test factors on operation efficiency.

3.5.1 Forward speed on the fragmentation pattern of wheat straw-soil aggregates

Setting the rotary tiller operating depth as 140 mm and the rotational speed of the cutter shaft as 280 r/min, the relationship between the influence of forward speed on the speed and force of wheat straw and each layer of soil was obtained. Under the same forward speed, there is no obvious difference between the speed and force of L_1, L_3, and L_5 wheat straw, as shown in Figure 18, but with the increase of forward speed, the disturbance degree of rotary tiller on wheat straw gradually decreases. As shown in Figure 19, because the rotary tillage knife carries out the rotary tillage and stubble removal operation from top to bottom, from far to near, the disturbance time for shallow soil is larger than that for middle and deep soil in turn. The degree of disturbance of each layer of soil in descending order is shallow soil>middle soil>deep soil. However, with the increase in forward speed, the disturbance degree of the rotary tiller on each layer of soil shows the same decreasing trend. The above phenomenon is mainly due to the same area of straw-soil aggregates by rotary tillage knife operation to reduce the time of disturbance, resulting in a lower degree of disturbance of straw-soil aggregates.

3.5.2 Working depth on the fragmentation pattern of wheat straw-soil aggregates

Setting the rotary tiller forward speed as 1 km/h and the rotational speed of the cutter shaft as 280 r/min, the relationship between the influence of the working depth on the speed and force of the wheat straw and soil was obtained. At the same operating depth, there is no obvious difference between the speed and force of L_1, L_3, and L_5 wheat straw, as shown in Figure 20. But as the working depth increases, the degree of disturbance of L_1, L_3, and L_5 wheat straw gradually increases, and the speed and force changes show an upward trend. As shown in Figure 21, at the same working depth, the degree of disturbance of each layer of soil by the rotary plough blade was in the following order: shallow soil>middle soil>deep soil, and the degree of disturbance of soil increases progressively with the working depth. The above phenomenon is mainly due to the increase in the disturbance time of the rotary tillage knife on shallow soil, as well as the increase in the initial kinetic energy of shallow soil. In contrast, wheat straw and middle and deep soil disturbance increased under the combined action of the rotary cutter and shallow soil.

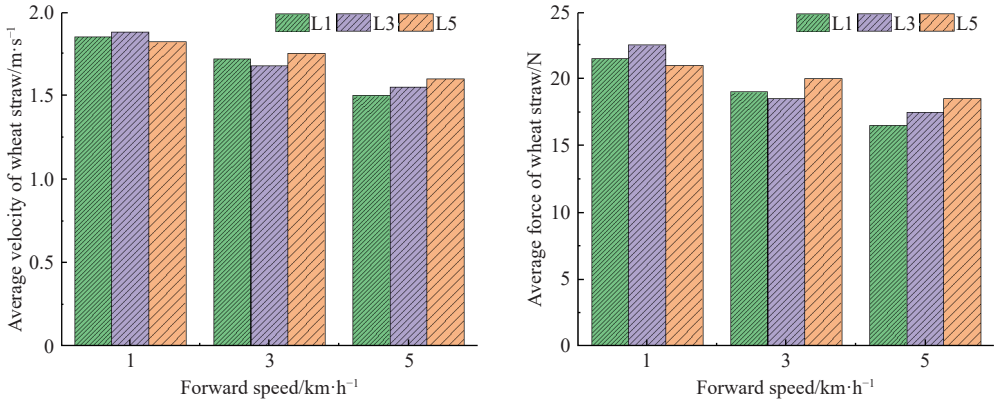

Figure 18 Mean velocity-force variation patterns of wheat straw

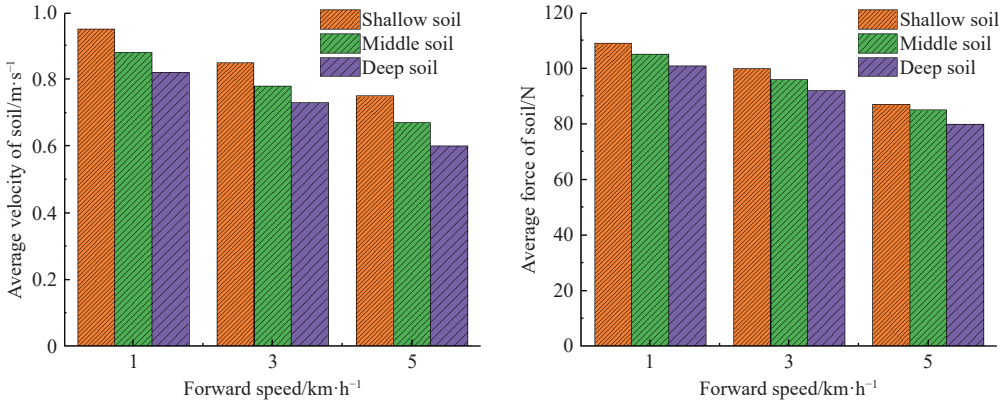

Figure 19 Influence law of forward speed on the velocity-force of soil

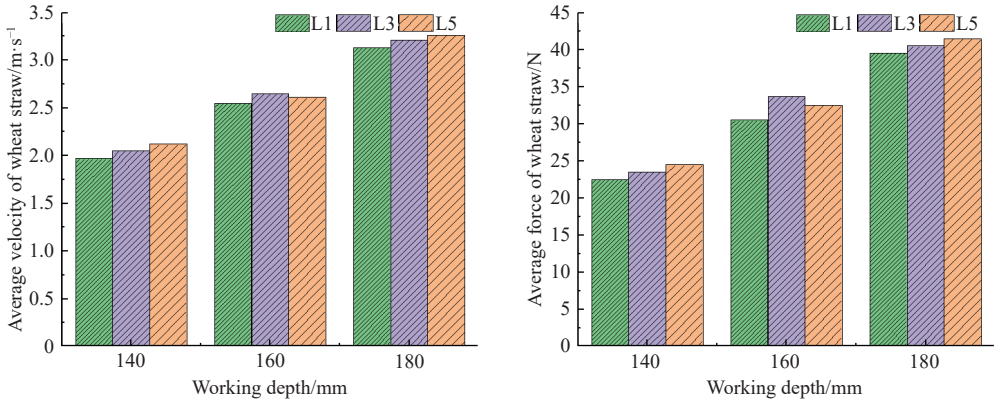

Figure 20 Influence law of working depth on the velocity-force of wheat straw

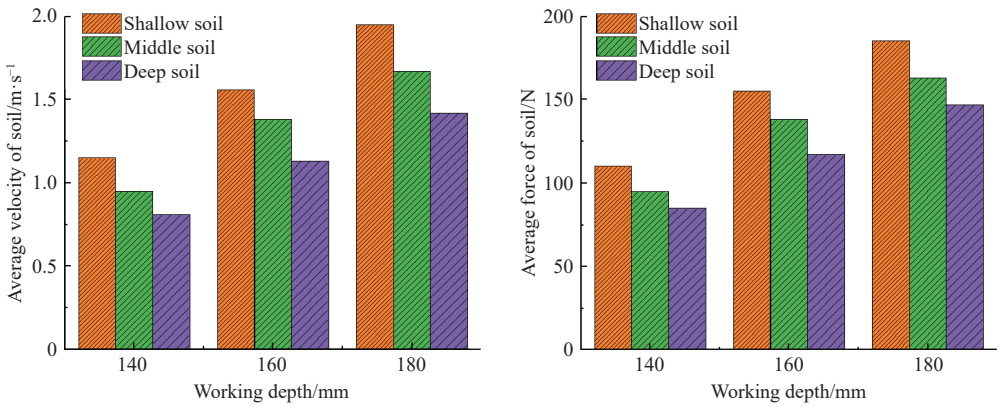

Figure 21 Influence law of working depth on the velocity-force of soil

3.5.3 Rotation speed on the fragmentation pattern of wheat straw-soil aggregates

Setting the forward speed of the rotary tiller as 1 km/h and the working depth as 140 mm, the relationship between the influence of the rotation speed on the speed and force of the wheat straw and each layer of soil was obtained. As shown in Figure 22, under the

same rotational speed of the cutter shaft, there is no obvious difference between the speed and force of L_1, L_3, and L_5 wheat straw. When the rotational speed increases, the disturbance level of L_1, L_3, and L_5 wheat straw gradually increases, but the degree of change is higher than that of the forward speed and operating depth for the degree of disturbance of straw. As shown in Figure 23, at the same rotational speed, the degree of disturbance of each layer of soil is in the following order: shallow soil>middle soil>deep soil, and the degree of disturbance of each layer of soil gradually increases with the increase of rotational speed. The above phenomenon is mainly due to the fact that with the increase of rotational speed of the cutter shaft, the failure area of wheat straw-soil aggregates under the action of rotary tillage knives increases, which strengthens the movement speed of wheat straw-soil moving along the tangent line of rotary tillage knives.

For mechanical characterization of wheat straw, combining previous research findings[47,48], when the rotational speed increases, the displacement and quantity of straw gradually increase. In this paper, when the rotational speed increases, the speed and force of the wheat straw also gradually increase, which is similar to previous findings. Relative to this paper, there is a lack of research on the kinetic properties and spatial homogeneity distribution of wheat straw. For mechanical characterization of soil, combining previous research findings[49,50], soil forward and side displacement in experiment increased with increasing rotational speed of blade, and the displacement of shallow soil was the largest; then middle soil and deep soil had the minimum displacement. This is consistent with the findings of the soil velocity and stress in this paper. In addition to this, this paper also investigates the relationship between the mechanical properties of soil under different parameters.

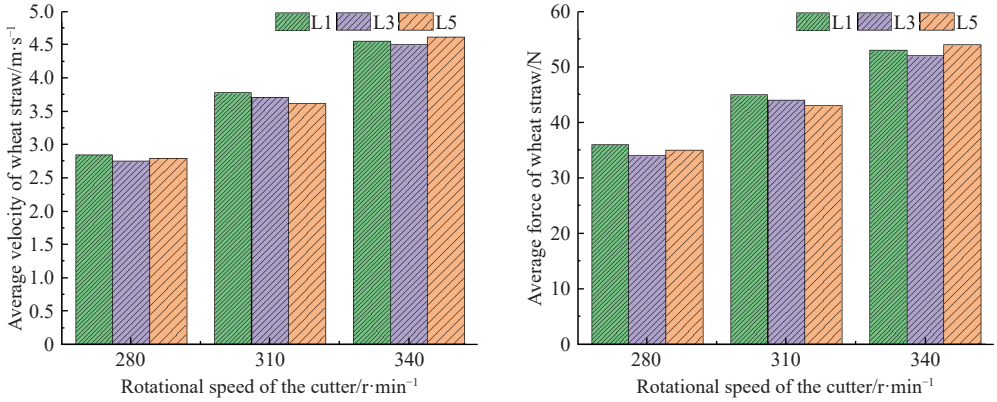

Figure 22 Influence law of rotation speed on the velocity-force of wheat straw

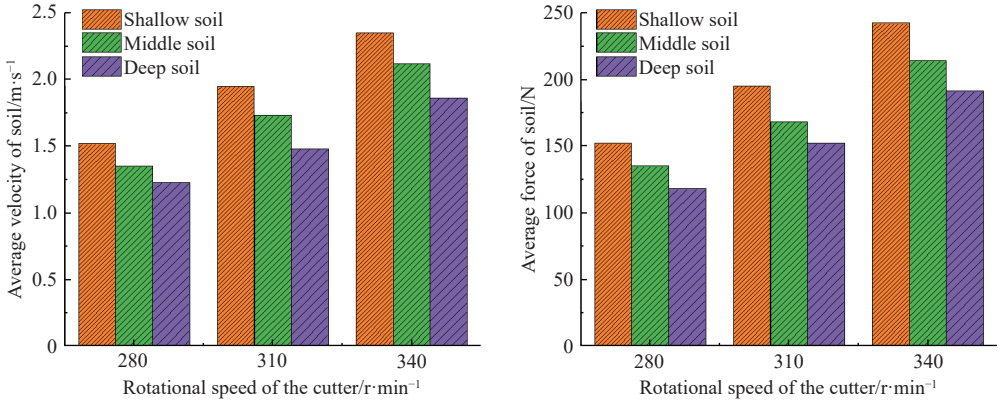

Figure 23 Influence law of rotation speed on the velocity-force of soil

3.6 Experimental optimization and analysis

3.6.1 Test factors codes

Since wheat straw-soil speed and force are positively correlated, in order to investigate the best combination of rotary tiller forward speed, operating depth, and cutter shaft rotational speed for wheat straw-soil agglomerate perturbation law, this paper takes the wheat straw speed Y_1 and the soil speed Y_2 as the experimental targets. It takes the forward speed A, working depth B, and rotation speed C as experimental factors, and applies Design-Expert to set up the combination test, as listed in Table 7.

Table 7 Factor coding table

Categorization	Symbol	–1	0	1
Forward speed/km·h^{-1}	A	1	3	5
Working depth/mm	B	140	160	180
Rotational speed of the cutter/r·min^{-1}	C	280	310	340

3.6.2 Results and analysis

The analysis of variance and regression coefficient significance of wheat straw speed Y_1 and soil speed Y_2 with test factors A, B, and C was carried out in conjunction with Design-Expert, and the results of the analysis of variance of wheat straw velocity Y_1 and soil velocity Y_2 were obtained, as listed in Table 8.

3.6.3 Analysis of the influence of different factors on wheat straw speed

As listed in Table 9, the ANOVA of wheat straw velocity Y_1 was obtained, in which the p-value of the regression model is less than 0.01, the misfit term is 0.0806>0.05, and the coefficient of determination is 0.9787. From the table, the primary term coefficients A, B, and C, the interaction term coefficient BC, and the secondary term coefficients A^2 and B^2 had highly significant effects on wheat straw velocity Y_1, and the interaction term coefficient AB and the secondary term coefficient C^2 had significant effects on

Table 8 Discrete element simulation test results

Serial No.	Factor			Y_1/m·s^{-1}	Y_2/m·s^{-1}
	A	*B*	*C*		
1	–1	–1	0	3.57	1.74
2	1	–1	0	3.26	1.42
3	–1	1	0	3.84	1.93
4	1	1	0	3.65	1.82
5	–1	0	–1	3.21	1.48
6	1	0	–1	2.92	1.14
7	–1	0	1	3.64	1.73
8	1	0	1	3.21	1.54
9	0	–1	–1	3.17	1.28
10	0	1	–1	3.54	1.68
11	0	–1	1	3.78	1.72
12	0	1	1	3.84	1.95
13	0	0	0	3.46	1.63
14	0	0	0	3.38	1.68
15	0	0	0	3.42	1.65
16	0	0	0	3.45	1.67
17	0	0	0	3.46	1.63

wheat straw velocity Y_1. The effects of each test factor on the significance of wheat straw velocity were, in descending order: rotational speed of the cutter>forward speed>working depth. The regression equation of wheat straw velocity Y_1 was obtained by combining with ANOVA:

$$Y_1 = 3.43 - 0.15A + 0.14B + 0.20C + 0.030AB - 0.035AC - 0.078BC - 0.096A^2 + 0.24B^2 - 0.093C^2 \quad (12)$$

Combined with Design-Expert analysis, the surface plots of the response of each test factor for the test indices of wheat straw velocity were obtained, as shown in Figure 24. For wheat straw velocity Y_1, setting the rotational speed as 310 r/min, as is shown in Figure 24a, the interaction of working depth and forward speed was obtained. Setting forward speed as a fixed factor, when the forward speed is certain, the wheat straw velocity increases with the increase of working depth. Setting working depth as a fixed factor, the wheat straw velocity decreases with the increase of forward speed.

Setting the working depth as 160 mm, the rotational speed of the cutter and forward speed interact as shown in Figure 24b. Setting forward speed as a fixed factor, the wheat straw velocity increases with the increase of the rotational speed of the cutter. Setting working depth as a fixed factor, the wheat straw velocity decreases with the increase of the forward speed.

Table 9 Wheat straw velocity analysis of variance

Source	Sum of squares	Degrees of freedom	Mean square	*F*	*p*
Model	1.01	9	0.11	35.70	<0.0001
A	0.19	1	0.19	59.48	<0.0001
B	0.15	1	0.15	47.48	<0.0001
C	0.33	1	0.33	106.18	<0.0001
AB	3.6×10^{-3}	1	3.6×10^{-3}	1.15	0.3189
AC	4.9×10^{-3}	1	4.9×10^{-3}	1.57	0.2509
BC	0.024	1	0.024	7.68	0.0276
A^2	0.039	1	0.039	12.34	0.0098
B^2	0.25	1	0.25	78.67	<0.0001
C^2	0.037	1	0.037	11.71	0.0111
Residual	0.022	7	3.128×10^{-3}		
Lack of fit	0.017	3	5.725×10^{-3}	4.85	0.0806
Pure error	4.72×10^{-3}	4	1.180×10^{-3}		
Sum	1.01	9	0.11	35.70	<0.0001

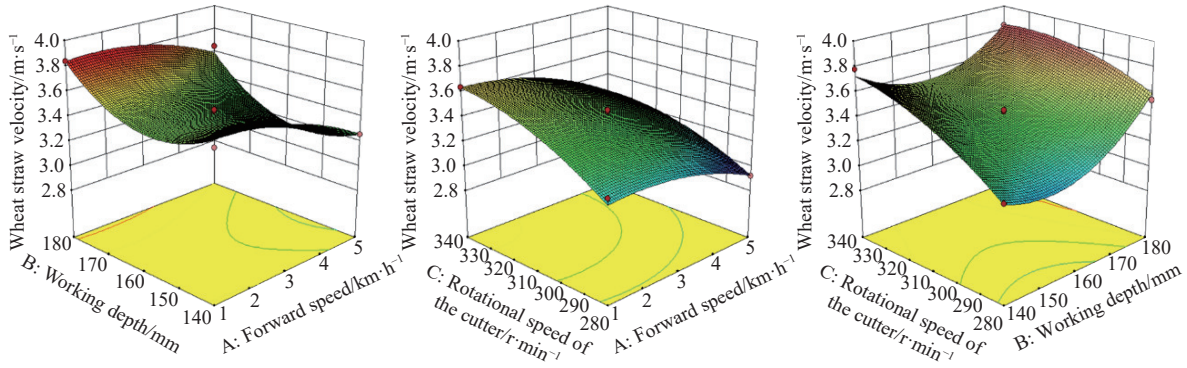

a. Rotational speed is 310 r/min b. Working depth is 160 mm c. Forward speed is 3 km/h

Figure 24 Relationship between the effects of test factors on soil velocity

Setting the forward speed to 3 km/h, the interaction between the rotational speed of the cutter and the working depth is shown in Figure 24c. Setting working depth as a fixed factor, the wheat straw velocity increases with the increase of rotational speed of the cutter. Setting rotational speed as a fixed factor, the wheat straw velocity increases with the increase of the working depth.

3.6.4 Relationship between the effects of different test factors on soil velocity

As listed in Table 10, the ANOVA of soil velocity Y_2 was obtained, in which the *p*-value of the regression model is less than 0.01, the misfit term is 0.4116>0.05, and the coefficient of determination is 0.9943. The primary term coefficients *A*, *B*, and *C*, the interaction term coefficients *AB* and *BC*, and the secondary term coefficients A^2, B^2, and C^2 had highly significant effects on soil velocity Y_2, and the interaction term coefficient *AC* had significant effects on soil velocity Y_2. The effects of each test factor on the significance of soil speed were, in descending order: rotational speed of the cutter>working depth>forward speed. The regression equation on soil speed Y_2 was obtained by combining with ANOVA:

$$Y_2 = 1.65 - 0.12A + 0.15B + 0.17C + 0.052AB + 0.038AC - 0.042BC - 0.055A^2 + 0.13B^2 - 0.12C^2 \quad (13)$$

As shown in Figure 25, combined with Design-Expert analysis, the surface plots of the response of each test factor for the test indices of soil velocity were obtained. As shown in Figure 25a, for

Table 10 Soil velocity analysis of variance

Source	Sum of squares	Degrees of freedom	Mean square	F	p
Model	0.70	9	0.078	136.60	<0.0001
A	0.12	1	0.12	202.61	<0.0001
B	0.19	1	0.19	327.225	<0.0001
C	0.23	1	0.23	406.63	<0.0001
AB	0.011	1	0.011	19.39	0.0031
AC	5.625×10^{-3}	1	5.625×10^{-3}	9.89	0.0163
BC	7.225×10^{-3}	1	7.225×10^{-3}	12.71	0.0092
A^2	0.013	1	0.013	22.20	0.0022
B^2	0.071	1	0.071	125.63	<0.0001
C^2	0.066	1	0.066	115.25	<0.0001
Residual	3.980×10^{-3}	7	5.686×10^{-4}		
Lack of fit	1.900×10^{-3}	3	6.333×10^{-4}	1.22	0.4116
Pure error	2.080×10^{-3}	4	5.200×10^{-4}		
Sum	0.70	9	0.078	136.60	<0.0001

soil velocity Y_2, when the rotational speed is 310 r/min, the interaction of working depth and forward speed was obtained. Setting forward speed as a fixed factor, the soil velocity increases with the increase of the working depth; setting working depth as a fixed factor, the soil velocity decreases with the increase of the forward speed.

As shown in Figure 25b, when the working depth is 160 mm, the interaction between the rotational speed of the cutter and forward speed was obtained. Setting forward speed as a fixed factor, the soil velocity increases with the increase of the rotational speed of the cutter; setting working depth as a fixed factor, the soil velocity decreases with the increase of the forward speed.

As shown in Figure 25c, when the forward speed is 3 km/h, the interaction between rotational speed of the cutter and working depth was obtained. Setting working depth as a fixed factor, the soil velocity increases with the increase of rotational speed of the cutter; setting rotational speed as a fixed factor, the soil velocity increases with the increase of working depth.

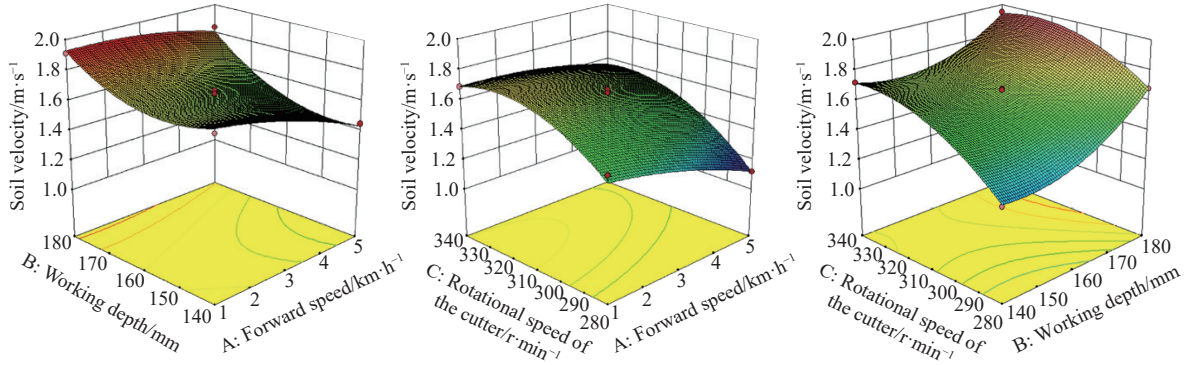

a. Rotational speed is 310 r/min b. Working depth is 160 mm c. Forward speed is 3 km/h

Figure 25 Relationship between the effects of test factors on soil velocity

3.7 Experimental optimization and validation

To further analyze the mechanism of soil fragmentation and straw mulching in saline soils, enhance the crushing rate of wheat straw-soil agglomerates, and improve the burial rate of wheat straw, the experimental factors were designed and optimized. According to the range of values of each test factor, this paper establishes an objective function with the constraints of rotational speed, forward speed, and working depth with the optimization objective of improving the speed of wheat straw and soil during the test.

$$\begin{cases} \max Y_1 \\ \max Y_2 \\ \text{s.t.} \begin{cases} 1\ \text{km/h} \le A \le 5\ \text{km/h} \\ 140\ \text{mm} \le B \le 180\ \text{mm} \\ 280\ \text{r/min} \le C \le 340\ \text{r/min} \end{cases} \end{cases} \tag{14}$$

Using Design-Expert post-processing optimization to solve the objective function, the rotary tiller optimal working parameters were obtained: forward speed is 2.02 km/h, working depth is 178.83 mm, and rotational speed is 324.94 r/min. Meanwhile, the wheat straw speed was 3.86 m/s and soil speed was 1.96 m/s. To validate the accuracy of the experimental results, the above optimal working parameters were imported into the discrete element model of the rotary tiller, five repetitive tests were conducted, and the results were averaged, upon which the velocity of wheat straw was 3.93 m/s and the soil velocity was 1.83 m/s. The maximum error was 6.63%, which indicated the accuracy of the test results.

4 Performance analysis of rotary tillers in field operations

4.1 Preparation for field trials

The performance test was conducted in June 2023 at the saline soil test and demonstration base of the Yellow River Delta (Figure 26). The basic physical properties of the soils were obtained prior to the test with the soil water content at 12%-16%, the soil firmness at 900-1200 kPa in depth of 0-210 mm, and the stubble height of wheat straw at 7-12 cm. Combining simulation test results and actual operational requirements, the forward speed is set at 2.2 km/h, working depth at 178.5 mm, and rotational speed of the cutter shaft at 325 r/min.

Figure 26 Field trial of layered stubble and crushing soil rotary tillage

Since traditional test methods cannot measure the kinetic properties of wheat straw-soil in the actual operation process, the soil fragmentation rate Y_3 and the wheat straw return rate Y_4 can characterize the velocity and force changes of wheat straw-soil from the side. At the same time, rotary tiller tillage depth stability can evaluate the performance of rotary tillage and stubble removal, which can reduce power consumption. This paper expresses the tillage depth stability of rotary tiller operation in terms of tillage depth stability Y_5.

The measurement of soil fragmentation rate refers to the Chinese standard (GB/T 5668-2017), and the soil blocks in the area after the operation were divided into three grades of less than 4 cm, 4-8 cm, and more than 8 cm according to their longest side. The percentage of soil blocks with a side length of less than 4 cm among the total cultivated soil blocks is the soil fragmentation rate, which was calculated by randomly choosing 10 measurement areas for the test:

$$Y_3 = \frac{m_a - m_3}{m_a} \times 100\% \tag{15}$$

where, Y_3 is the soil fragmentation rate, %; m_a is the total mass of soil blocks, g; m_3 is the mass of soil blocks with the longest side greater than 4 cm, g.

To ensure the precision of the test, 10 groups of 1.0 m×1.0 m test areas were selected by the five-point sampling method, and the test results were averaged:

$$Y_4 = \left(1 - \frac{m_2}{m_1}\right) \times 100\% \tag{16}$$

where, Y_4 is the wheat straw return rate, %; m_1 is the total mass of straw in the experimental area before the experiment, g; m_2 is the total mass of straw in the experimental area after the experiment, g.

In order to ensure the accuracy of the test, 10 groups of 1.5 m×1.5 m test areas were selected by the five-point sampling method, and the test results were averaged:

$$Y_5 = \left(1 - \frac{\sqrt{\sum_{i=1}^{N}(a_i - a)^2 / N}}{\sum_{i=1}^{N} a_i / N}\right) \times 100\% \tag{17}$$

where, Y_5 is the tillage depth stability, %; N is the amount of measurement points; a is working depth of rotary tillers, mm; a_i is cultivation depth value at location i, mm.

4.2 Preparation for field trials

As shown in Table 11, for the soil fragmentation, the maximum value of the soil fragmentation rate is 92.57%, the minimum value is 91.18%, and the average value is 91.85%. For the wheat straw return rate, the maximum value is 91.65%, the minimum value is 90.47%, and the average value is 91.09%. For the tillage depth stability, the maximum value is 92.28%, the minimum value is 89.45%, and the average value is 91.12%.

Table 11 Field trial results

No.	Soil fragmentation rate/%	Wheat straw return rate/%	Tillage depth stability/%
1	91.18	90.85	89.45
2	92.57	91.24	91.79
3	91.47	90.47	92.28
4	92.26	91.65	90.45
5	91.75	91.24	91.64
Average value	91.85	91.09	91.12

According to Chinese standards (NT/Y 499-2013 Rotary Tiller Operation Standard) and (GB/T5668-2017 Rotary Tiller Standard), the straw return rate should be more than 80%, the soil fragmentation rate more than 80%, and the tillage depth stability more than 85%. The results of the field performance test show that the soil fragmentation rate is 91.85%, the straw return rate is 91.09%, and the tillage depth stability is 91.12%, indicating that the designed rotary tiller can effectively improve the wheat straw-soil aggregate crushing and burying and satisfy the basic requirements for the preparation of high-performance seed beds in saline and alkaline land.

To verify the performance of the layered stubble and soil crushing rotary tillage knife, a comparative test was conducted with a common rotary tiller IT245. The forward speed was set at 2.0 km/h, working depth at 179 mm, and rotational speed of the cutter shaft at 324 r/min; the test results are listed in Table 12. For soil fragmentation rate, layered stubble rotary tillage knife is 6.99% higher than IT245; for wheat straw return rate, layered stubble rotary tillage knife is 8.68% higher than IT245; for tillage depth stability, layered stubble rotary tillage knife is 9.20% higher than IT245.

Table 12 Results of comparative field trials

Test indicators	Layered stubble rotary tillage knife	IT245
Soil fragmentation rate/%	91.85	85.43
Wheat straw return rate/%	91.09	83.17
Tillage depth stability/%	91.12	82.74

5 Conclusions

For the problems of low soil crushing rate and straw burying rate during the preparation of saline seed bed, this study designed a layered stubble and soil crushing rotary tillage knife, which is divided into the upper short-edged stubble knife and the lower long-edged soil crushing knife. By analyzing the rotary tillage knife-straw-soil interaction mechanism, the optimal structural parameters and working parameters of the rotary tillage knife were determined.

To analyze the soil-straw displacement pattern and mechanical properties during rotary tillage process, an analysis of the soil-straw movement behavior of saline soil under different working parameters of rotary tiller was conducted. In addition, the single-factor test was carried out with the movement speed and force of saline soil-straw aggregate as the test indices, and the dynamic process of saline soil-straw aggregate crushing was systematically investigated from a microscopic point of view. Meanwhile, to further analyze the mechanism of soil fragmentation and straw mulching in saline soils, the rotary stubble test was carried out with soil fragmentation rate, straw burial rate, and tillage depth stability as the test indices. The results show that the soil fragmentation rate is 91.85%, the straw mulching rate is 91.09%, and the tillage depth stability is 91.12%, which indicates that the designed rotary tiller can effectively improve the soil crushing and straw mulching in saline and alkaline land, and satisfy the basic requirements for the preparation of high-performance seed beds in saline and alkaline land.

In future research work, this rotary tiller can be used to verify the quality and performance of cultivation in other saline alkali land areas in China, improve machine adaptability, and further explore soil cutting performance and drag reduction power consumption models to ensure soil cutting throwing performance in saline alkali land and improve machine cultivation performance. At the same time, an intelligent decision-making and control system needs to be

added to achieve intelligent operation quality monitoring and realize intelligent cultivation operations.

Acknowledgements

We acknowledge that this work was financially sponsored by the Shandong Province Key R&D Program (Major Science and Technology Innovation Project) (Grant No. 2021CXGC010813), Saline Land Tillage Mechanization Equipment Research and Development, Manufacturing and Popularization of Application (Grant No. NJYTHSD-202314), Key R&D Program of Shandong Province (Science and Technology Demonstration Project) (Grant No. 2024SFGC0405), the National Key Research and Development Program (Grant No. 2022YFD2300101), Creation of Key Components of Equipment for Efficient Cultivation of Saline and Alkaline Land (Grant No. Y20240055), and Research and Development of High Quality Tillage and Compound Operation Technology and Equipment for Saline and Alkaline Land (Grant No. WSR2023093).

[References]

[1] Wang B, Dou W J, Chen J, Chen J W, Lai J B. Characteristics of spatial-temporal dynamics of soil salinity in the Yellow River Delta and zoning and high quality utilization of saline soil. Geosciense, 2025; 39(2): 070.

[2] Chen M. Evaluation of soil quality and analysis of obstacle factors in saline-alkali land in the Yellow River Delta-A case study of the agricultural high-tech industry demonstration area of the Yellow River. Shandong: Ludong University, 2023. DOI: 10.27216/d.cnki.gysfc.2023.000199. (in Chinese)

[3] Li L, Fan L Q, Wu X, Zhang Y H. Effects of straw returning to field on physical properties, enzyme activity of saline-alkali soil and yield of oil sunflower. Acta Agric. Boreali-Occident. Sin, 2019; 28(12): 1997–2004.

[4] Zhu W, Gu S, Jiang R, Zhang X, Hatano R. Saline–alkali soil reclamation contributes to soil health improvement in China. Agriculture, 2024; 14: 1210.

[5] Du Y Q, Liu X F, Zhang L, Zhou W. Drip irrigation in agricultural saline-alkali land controls soil salinity and improves crop yield: Evidence from a global meta-analysis. Sci. Total Environ, 2023; 880: 163226.

[6] Zhang Y T, Hou K, Qian H, Gao Y Y, Xiao S, Tang S Q, et al. Characterization of soil salinization and its driving factors in a typical irrigation area of Northwest China. Sci. Total Environ, 2022; 837: 155808.

[7] Li J G, Pu L J, Han M F, Zhu M, Zhang R S, Xiang Y Z. Soil salinization research in China: Advances and prospects. J. Geogr. Sci, 2014; 24: 943–960.

[8] Cuevas J, Daliakopoulos I N, Del Moral F, Hueso J J, Tsanis I K. A Review of soil-improving cropping systems for soil salinization. Agronomy, 2019; 9: 295.

[9] Zhang C L, Xia J F, Zhang J M, Zhou H, Zhu Y H, Wang J W. Design and experiment of knife roller for six-head spiral straw returning cultivator. Transactions of the CSAM, 2019; 50(3): 25–34. (in Chinese)

[10] Yang W, Xiao X, Pan R, Guo S, Yang J. Numerical simulation of spiral cutter–soil interaction in deep vertical rotary tillage. Agriculture, 2023; 13: 1850.

[11] Yang Y, Long Y, Li S, Liu X. Straw return decomposition characteristics and effects on soil nutrients and maize yield. Agriculture, 2023; 13: 1570.

[12] Gao Y L. Simulation optimization and experimental study of a counter-rotating straw returning machine based on the discrete element method. Anhui Agricultural University, 2019. DOI: 10.26919/d.cnki.gannu.2019.000428. (in Chinese)

[13] Wang L J, Zhou B, Wan C, Zhou L. Structural parameter optimization of a furrow opener based on EDEM software. Int J Agric & Biol Eng, 2024; 17(3): 115–120.

[14] Zhang X Y, Hu X, Zhang L X, Kheiry A N O. Simulation and structural parameter optimization of rotary blade cutting soil based on SPH method. Int J Agric & Biol Eng, 2024; 17(3): 82–90.

[15] Yang Y W, Tong J, Ma Y H, Jiang X H, Li J G. Design and testing of a bionic rotary tillage knife featuring the multi-toe structure of the mole. Transactions of the CSAE, 2019; 35(19): 37–45.

[16] Habibi A J, Surendra S. Optimization and evaluation of rotary tiller blades: Computer solution of mathematical relations. Soil Tillage. Res, 2009; 106: 1–7.

[17] Saunders C, Ucgul M, Godwin R J. Discrete element method (DEM) simulation to improve performance of a mouldboard skimmer. Soil Tillage. Res, 2021; 205: 104764.

[18] Azimi-Nejadian H, Karparvarfard S H, Naderi-Boldaji M. Weed seed burial as affected by mouldboard design parameters, ploughing depth and speed: DEM simulations and experimental validation. Biosyst. Eng., 2022; 216: 79–92.

[19] Torotwa I, Ding Q S, Makange N R, Liang L, He R Y. Performance evaluation of a biomimetically designed disc for dense-straw mulched conservation tillage. Soil Tillage. Res, 2021; 212: 105068.

[20] Farid Eltom A E, Ding W M, Ding Q D, Tagar A A, Talha Z, Gamareldawla. Field investigation of a trash-board, tillage depth and low speed effect on the displacement and burial of straw. Catena, 2015; 133: 385–393.

[21] Huang Y X, Gao P Y, Zhang Q K, Shen H, Zhu R X, Shi J T. Design and experiment of grass soil separation device with combination of stubble cutting and grass guiding used for no-till planter. Transactions of the CSAM, 2020; 51(5): 67–78.

[22] Gu J, Ji C Y, Fang H M, Zhang Q Y, Hua F L, Zhang C. Experimental analysis of soil and straw displacement after up-cut and down-cut rotary tillage. Transactions of the CSAM, 2016; 47(5): 21–26.

[23] Xu G M, Ding Q S, Wang X C, Liang L, He R Y, Chen X X. Analysis of straw displacement and burying effect in straw-soil-rotary tiller interaction. Transactions of the CSAM, 2022; 53(7): 23–29.

[24] Zhu Y H. Research on the working mechanism and consumption reduction of rotary burial blade roller for straw returning. Huazhong Agricultural University, 2020. DOI: 10.27158/d.cnki.ghznu.2020.000926. (in Chinese)

[25] Song Z H, Li H, Yan Y F, Tian F Y, Li Y D, Li F D. Calibration method of contact characteristic parameters of soil in mulberry field based on unequal-diameter particles DEM theory. Transactions of the CSAM, 2022; 53(6): 21–33.

[26] Liu D J, Gong Y, Zhang X J, Yu Q X, Zhang X, Chen X, et al. EDEM simulation study on the performance of a mechanized ditching device for codonopsis planting. Agriculture, 2022; 12(8): 1238.

[27] Guo Z Y, Lu C Y, He J, Wang Q J, Li H W, Zhai C K. Design and experiment of active spiral pushing straw row-sorting device. Agriculture, 2024; 14(1): 137.

[28] Geng Y L, Wang X L, Zhong X K, Zhang X C, Chen K, Wei Z C, et al. Design and optimization of a soil-covering device for a corn no-till planter. Agriculture, 2022; 12(8): 1218.

[29] Zheng S, Lu T, Liu J, Tian Y, Han M M, Tai M H, et al Discrete element-based design of a high-speed rotary tiller for saline-alkali land and verification of optimal tillage parameters. Agriculture, 2025; 15(3): 269.

[30] Zheng K, He J, Li H W, Zhao H B, Hu H N, Liu W Z. Design and testing of a counter-rotating deep pine combine tiller. Transactions of the CSAM, 2017; 48(8): 61–71.

[31] Liu J, Lu T, Zheng S, Tian Y, Han M M, Tai M, et al. Parameter calibration method for discrete element simulation of soil–wheat crop residues in saline-alkali coastal land. Agriculture, 2025; 15(2): 129.

[32] Xu G M, Wang X C, He R Y, Ding Q S. Performance evaluation of rotary tillage straw returning based on composite indicators and measurement techniques. Transactions of the CSAM, 2022; 53(2): 58–67.

[33] Liu G Y. Research on mechanism and device for rotary tillage to reduce adhesion and increase detachment under the sticky soil condition of rice stubble fields in the paddy-upland rotation area. Huazhong Agricultural University, 2024. DOI: 10.27158/d.cnki.ghznu.2024.000199.

[34] Lee K S, Park S H, Park W Y, Lee C S. Strip tillage characteristics of rotary tiller blades for use in a dryland direct rice seeder. Soil Tillage. Res., 2003; 71: 25–32.

[35] Sun J Y, Wang Y M, Ma Y H, Tong J, Zhang Z J. DEM simulation of bionic subsoilers (tillage depth >40 cm) with drag reduction and lower soil disturbance characteristics. Advances in Engineering Software, 2018; 119: 30–37.

[36] Pirchio M, Fontanelli M, Labanca F, Sportelli M, Frasconi C. Energetic aspects of turfgrass mowing: Comparison of different rotary mowing systems. Agriculture, 2019; 9: 178.

[37] Zhang Y F, Liu J, Yuan W, Zhang R H, Xi X B. Multiple leveling for paddy field preparation with double axis rotary tillage accelerates rice growth and economic benefits. Agriculture, 2021; 11: 1223.

[38] Ding W M, Wang Y H, Peng S Z. Performance analysis of forward and

reverse rotary tiller and comparative cutting torque test. Nanjing Agric. Univ, 2001; 1: 113–117.

[39] Zhang J. Research on energy-saving technology of down-cut deep-rotary-tillage rotary tiller. Nanjing Institute of Agricultural Mechanization Ministry of Agriculture and Rural Affairs, 2021. DOI: 10.27630/d.cnki.gznky.2021.000889. (in Chinese)

[40] Zhao H B, Huang Y X, Liu Z D, Liu W Z, Zheng Z Q. Applications of discrete element method in the research of agricultural machinery: A review. Agriculture, 2021; 11: 425.

[41] Han L J, Yuan W, Yu J J, Jin J J, Xie D S. Simulation and experiment of spiral soil separation mechanism of compound planter based on discrete element method (DEM). Agriculture, 2022; 12: 511.

[42] Ucgul M, Fielke J M, Saunders C. 3D DEM tillage simulation: Validation of a hysteretic spring (plastic) contact model for a sweep tool operating in a cohesionless soil. Soil Tillage. Res., 2014; 144: 220–227.

[43] Magalhães P S G, Bianchini A, Braunbeck O A. Simulated and experimental analyses of a toothed rolling coulter for cutting crop residues. Biosyst. Eng., 2007; 96: 193–200.

[44] Jan D P, Gemmina D E, Daniel V F R, Adam B, Wim M C. Calibration of DEM material parameters to simulate stress-strain behavior of unsaturated soils during uniaxial compression. Soil Tillage. Res., 2019; 194: 104303–104312.

[45] Rahman S, Chen Y. Laboratory investigation of cutting forces and soil disturbance resulting from different manure incorporation tools in a loamy sand soil. Soil Tillage. Res, 2001; 58: 19–29.

[46] Zhang Z G, Xue H T, Wang Y C, Xie K T, Deng Y X. Design and experiment of panax notoginseng bionic excavating shovel based on EDEM. Transactions of the CSAM, 2022; 53(5): 100–111.

[47] He R Y, Duan Q F, Chen X X, Xu G M, Ding Q S. DEM analysis of spatial distribution quality of rotary tillage straw returning. Transactions of the CSAM, 2022; 53(6): 44–53.

[48] Xu G M, Xie Y X, Matin M A, He R Y, Ding Q S. Effect of straw length, stubble height and rotary speed on residue incorporation by rotary tillage in intensive rice–wheat rotation system. Agriculture, 2022; 12: 222.

[49] Fang H M, Ji C Y, Ahmed A T, Zhang Q Y, Guo J. Simulation analysis of straw movement in straw-soil-rotary blade system. Transactions of the CSAM, 2016; 47(1): 60–67.

[50] Fang H M, Ji C Y, Farman A C, Guo ., Zhang Q Y, Chaudhry A. Analysis of soil dynamic behavior during rotary tillage based on distinct element method. Transactions of the CSAM, 2016; 47(3): 22–28. (in Chinese)